ARC Geophysical Research

A Paradigm Shift in Colloid Filtration: Upscaling from Grain to Darcy Scale

Bashar M. Al-Zghoul*[1], William P. Johnson[2], and Diogo Bolster[1]

[1]University of Notre Dame, Department of Civil & Environmental Engineering & Earth Science
[2]University of Utah, Department of Geology & Geophysics

Abstract

This study introduces a novel theoretical model for upscaling colloid transport from the grain scale to the Darcy scale under both favorable and unfavorable conditions. The model integrates colloid interception history, where an interception occurs when colloids enter the near-surface zone within 200 nm of a collector, to capture the traditional exponential retention profile, as well as the anomalous, non-exponential behaviors observed under unfavorable conditions. The development of this theoretical model is based on a two-stage framework: first, upscaling from the grain scale to the single-interception scale, followed by upscaling from the single-interception scale to the Darcy scale. The initial stage addresses the distribution of colloids corresponding to a given interception order. The second stage focuses on the distribution of colloids across multiple interception orders. The key innovation of this work is the inclusion of the colloid removal process, where a fraction, denoted by α, is removed at each encountered interception, rather than with each grain passed, as specified by classical colloid filtration theory. Our model accounts for scenarios under unfavorable conditions wherein if α remains constant, the distribution is exponential, albeit shallower relative to favorable conditions. Additionally, the model considers cases where α varies with interceptions, leading to multi-exponential and non-monotonic retention profile shapes. In both scenarios, the proposed theoretical model offers a mathematical representation of colloid retention profiles under favorable and unfavorable conditions, including those exhibiting anomalous shapes.

Keywords: Colloids, Anomalous Transport, Upscaling, Retention Profiles, Multi-Exponential, Nonmonotonic, Unfavorable Conditions

*Corresponding Author
E-mail addresses: balzghou@nd.edu
doi: https://10.5149/ARC-GR.1582

1 Introduction

The transport of colloidal particles, typically ranging in size from 10 nm to 10 μm, in complex environmental systems has garnered significant interest across various research communities [23, 29]. A colloid retention profile (RP), defined here as the number of retained colloids in the hosting medium as a function of distance, has been widely used as a key indicator of the spread of colloids within environmental systems [23, 29]. In laboratory experiments conducted using identical colloids under unfavorable conditions, where a repulsive energy barrier is present and sufficiently strong to prevent any physical contact between the colloids and the grains of the hosting medium, RPs exhibited two distinct shapes, multi-exponential and nonmonotonic, that deviate from the exponential RPs typically observed under favorable conditions, where the repulsive energy barrier is either absent or negligible [5, 19, 20, 31]. This deviation highlights the complex interplay between hydrodynamic forces and near-surface interactions under unfavorable conditions. This underscores the need for further investigation to understand better and predict colloid transport and retention behavior in environmental systems.

Under favorable conditions, colloid transport can be effectively described by the advection-diffusion-reaction equation with a first-order reaction term to capture attachment processes [10]. This aligns with experimentally observed exponential RPs under favorable conditions [16, 20, 32], as explained by Colloid Filtration Theory (CFT) [35], which attributes loss of a fraction of colloids with each grain passed. Mechanistic models and empirical correlation equations, based on simplified geometries like the Happel Sphere-in-Cell, have been developed to predict these exponential RPs [15, 24, 26]. A key parameter derived from these models is the "collector efficiency" (η), which quantifies the proportion of colloids that intercept a collector to those approaching it. These models have reliably estimated η under various advection and diffusion scenarios, enabling its direct application in calculating the attachment rate constant under favorable conditions (k_f). Overall, CFT considers a constant fractional removal from the bulk fluid (outside the NSZ) with each grain passed, yielding an exponential decay of colloid population with distance.

In contrast, predicting anomalous RPs, characterized by multi-exponential or nonmonotonic shapes observed under unfavorable conditions, represents a significant challenge that still requires extensive investigation. Theoretically, the presence of a sufficiently large repulsive energy barrier under unfavorable conditions, from DLVO and/or extended DLVO theory, should prevent any colloid from attaching to the grains of the medium. One possible mechanism to explain colloid attachment under unfavorable conditions is the presence of local surface charge heterogeneity (heterodomains) on the surface of the hosting medium. These sufficiently large heterodomains can locally eliminate the repulsive energy barrier, thereby allowing colloids to attach to the surface of the hosting medium. These heterodomains can locally eliminate the repulsive energy barrier, thereby allowing colloids to attach to the surface of the hosting medium [25, 27, 28]. In the development of models capable of predicting RPs under unfavorable conditions, one approach has been an upscaled two-population model, suggesting that colloid populations can be divided into fast- and slow-attaching subpopulations [11, 12]. In this model, fast-attaching subpopulations, representing a fraction α_1 of the total population, are assumed to attach at a favorable rate (k_f). In contrast, the slow-attaching subpopulations are described as attaching more slowly, governed by their interaction with grain surfaces through two exponential steps: the rate of entry into the near-surface zone (NSZ) via diffusion (k_{ns}) and the rate of attachment within the NSZ (k^*_{f2}). These rate parameters collectively describe colloid transport and retention under unfavorable conditions. The fast-attaching rate (k_f) corresponds to the rate observed under favorable conditions and can be directly calculated using classical filtration theory (CFT) correlation equations [10, 24]. Meanwhile, calculating k_{ns} and k^*_{f2} requires data from mechanistic trajectory simulations to parameterize the upscaled formulas [11]. A complementary approach estimates the rate coefficients from experimental data using an inverse modeling approach [34].

The notion that multiple rates govern the transport of identical individuals has remained a subject of debate, as it is not clear why identical colloids should behave differently. In this context, colloid transport under unfavorable conditions has been examined, emphasizing the influence of interception history on transport variability in porous media by [33] . Through pore-assembly simulations [1, 2], they classified attached colloids based on the number of grains they intercepted (entering their NSZ) before attachment. They introduced α as the fraction of colloids that attach upon interception and k_f as the attachment rate constant. Under favorable conditions, their findings indicated that nearly all colloids attach during their first interception ($\alpha \approx 1$) with the favorable attachment rate (k_f), thus replicating classical theories. Conversely, under unfavorable conditions, the attachment process was found to occur after multiple interceptions. They further categorized the attached population into single-interceptors, which are attached upon their first interception, and multi-interceptors, which are attached only after experiencing more than one interception. Their subsequent analysis of the spatial and temporal distribution of single- and multi-interception attachers in the bulk fluid revealed that the distributions for single-interception attachers followed an exponential shape. In contrast, those for multi-interception attachers followed a gamma distribution. Moreover, they found that the spatial and temporal distributions of single-interception attachers under unfavorable conditions exhibited the same rate (k_f) as those under favorable conditions. They also demonstrated that the self-convolution of the exponential distribution for single-interception attachers under unfavorable conditions yields the gamma distribution observed for multi-interception attachers. Additionally, it has been revealed that a constant fraction (α) is removed from the bulk fluid at each interception rather than at each grain passed (as described by the classical CFT) [33].

This observed trend in the bulk fluid motivated a new framework and the development of a novel upscaling approach to predict RPs and residence time distributions (RTDs). To this end, a general random walk model was proposed to utilize information from single-interception attachers to predict RPs and RTDs [3]. This model treats interception events as statistically independent and identically distributed (iid). By incorporating the appropriate α value and the favorable rate k_f, the model offers an efficient upscaling strategy for predicting colloid transport and retention under unfavorable conditions [3]. However, this approach was highly empirical in nature. While empirical frameworks are useful for predicting colloid RPs based on certain inputs, they do not provide the theoretical foundation necessary to fully describe the underlying mechanisms governing colloid transport and retention in porous media. Thus, the need for a more rigorous theoretical approach arises to better elucidate the interactions between colloids and the medium, particularly under unfavorable conditions where anomalous multi-exponential and nonmonotonic RPs emerge.

In this paper, we develop an theoretical model for upscaling colloid transport and retention in porous media, employing the observed trend in the bulk fluid [33], the concepts of the upscaled random walk model [3], and the principals of CFT [35] to develop an analytical framework capable of predicting full RPs under favorable and unfavorable conditions including those with multi-exponential and nonmonotonic shapes.

2 Model Formulation

Before developing our general model, we present an overview of the classical CFT upscaling approach, which has proven effective in predicting RPs under favorable conditions. Building on this foundation, we then propose a framework that involves upscaling from the grain scale to the single-interception scale, followed by a subsequent upscaling from the single-interception scale to the Darcy scale. This approach is designed to construct a general model capable of creating RPs both under favorable and unfavorable conditions.

2.1 Overview of the CFT Approach

As previously discussed, the CFT framework assumes that a constant fraction of colloids is removed from the bulk with each grain encountered, herein referred to as α_{CFT}. Figure 1, panel b, illustrates the traditional upscaling methodology employed by utilizing η and α_{CFT}. The parameter η can be determined through CFT correlation equations [15, 23, 24]. CFT assumes an exponential removal from the bulk with distance at a constant rate of k_f:

$$C(x) = C_o \exp\left(-\frac{k_f}{\langle v\rangle}x\right), \tag{1}$$

where C_o denotes the influent concentration, C represents the concentration at downstream distance x, and $\langle v\rangle$ is the average fluid velocity. In this framework, the concentration C_o is assumed to be sufficiently diluted such that it exerts a negligible influence on the flow conditions, and the colloids are considered significantly smaller than the average pore size. Given Eqn (1) and $C/C_o = (1-\alpha_{CFT}\eta)^{N_c}$ as shown in Figure 1, panel b, the attachment rate constant (k_f) can be represented by:

$$k_f = -\frac{N_c}{x}\langle v\rangle \ln(1-\alpha_{CFT}\eta), \tag{2}$$

N_c/x represents the number of grains passed within a specific transport distance and is related to grain diameter (d_c) and porosity (ϵ). An expression for N_c/x was developed based on Happel Sphere-in-Cell geometry as

$$\frac{N_c}{x} = \frac{3\,(1-\epsilon)^{1/3}}{2d_c}. \tag{3}$$

Substituting Eqn (3) into (2) gives:

$$k_f = \frac{3\,(1-\epsilon)^{1/3}}{2d_c}\langle v\rangle \ln(1-\alpha_{CFT}\eta). \tag{4}$$

Using the CFT upscaling strategy illustrated in Figure 1, panel b, k_f is expressed as a function of the product of η and α_{CFT}. This product is explicitly incorporated in Eqn (4). However, under favorable conditions, CFT assumes that all colloids encountering a grain will attach, implying that α_{CFT} is approximately equal to 1. It is important to note that, under favorable conditions, substituting $\alpha_{CFT} = 1$ into Eqn (4) will cause α_{CFT} to disappear from the equation. Nevertheless, it remains implicitly included, as CFT assumes that a constant fraction of colloids is removed with each grain passed. Although CFT has successfully predicted exponential RPs under favorable conditions using Eqn (1) with k_f from Eqn (4), it proves inadequate for predicting RPs under unfavorable conditions, particularly those exhibiting anomalous multi-exponential or nonmonotonic shapes [10, 23].

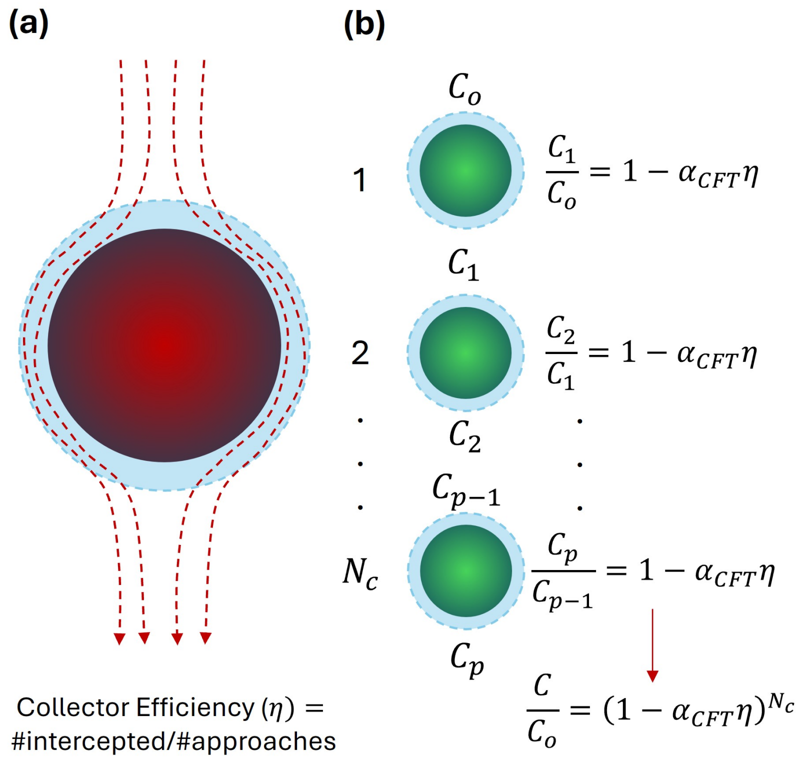

Figure 1: The conventional upscaling method, which utilizes the CFT approach [13], is based on the following parameters: C_o represents the influent concentration, C_p is the concentration after the colloid has passed through p grains, N_c denotes the number of grains the colloid has passed, η is the collector efficiency, and α_{CFT} is the constant fraction of colloids removed by each grain passed. (a) A schematic of a spherical grain illustrating intercepted colloid trajectories as they enter the NSZ. (b) Upscaling using the CFT approach, with a constant fractional removal (α_{CFT}) for each grain passed.

2.2 Upscaling from Grain Scale to Single-Interception Scale

Our upscaling strategy is structured into two distinct stages: (i) upscaling from the grain scale to the single-interception scale and (ii) upscaling from the single-interception scale to the Darcy scale. In the first stage, we characterize the transport of colloids from the bulk fluid to the NSZ without considering attachment processes. In the second stage, we integrate colloid attachment across successive interceptions. This section focuses on the first stage of our upscaling approach. In general, upscaling from the grain scale to the single-interception scale follows a conceptual framework similar to the CFT upscaling scheme presented in Figure 1, panel b. However, our focus here is on capturing the spatial distribution of colloids within a single-interception order while excluding attachment mechanisms at this stage. As a result, the delivery of colloids in the bulk fluid to the NSZ during a single-interception event can be described using the CFT upscaling scheme in Figure 1, panel b, with the removal term (α_{CFT}) omitted from the process. Consequently, the rate of colloid delivery to the NSZ is governed by Eqn (5), which remains independent of α_{CFT} and is analogous to the attachment rate constant under favorable conditions, incorporating the fraction intercepted per grain encountered:

$$k_f = \frac{3\,(1-\epsilon)^{1/3}}{2d_c}\langle v\rangle \ln(1-\eta). \tag{5}$$

This process is illustrated in Figure 2, panel a, where colloid transport is depicted as a sequence of interceptions, and the rate of colloid interception (within a single-interception order) is described by Eqn (5). This outcome is reasonable since the rate of delivery to the NSZ should not be influenced by near-surface interactions but rather governed solely by the bulk fluid delivery [3, 10, 33]. Therefore, the spatial distribution of colloids among each interception event is governed by Eqn (1) employing k_f from Eqn (5)

2.3 Upscaling from Single-Interception Scale to Darcy Scale

The bulk delivery process at a single-interception order corresponds to the initial upscaling stage described in §2.2. Subsequently, we seek to upscale from the single-interception order scale to the multi-interception orders (Darcy) scale. This transition is achieved by iterating the process occurring at the first stage multiple times (i.e., through successive interceptions), as illustrated in Figure 2, panel a. This iterative process exhibits scale invariance, as the same removal mechanism is applied across successive interception orders. At each interception order, a fraction α of the colloids is removed, as detailed in Figure 2, panel (b). Here, α is included at the interception scale rather than the grain scale. For instance, once all colloids experience their first interception, we define α as the fraction of intercepted colloids that attach, with $1 - \alpha$ representing the fraction that returns to the bulk and begins a new, independent trajectory toward the next interception. Under favorable conditions, most of the colloids should attach from their first interception, resulting in exponential RPs with a rate k_f and $\alpha \approx 1$ [33]. In contrast, under unfavorable conditions, colloid transport and deposition proceed through multiple interception events, with only a fraction of colloids attaching at each event (i.e., $\alpha < 1$), yielding RPs distinct from those observed under favorable conditions. Since the sole distinction between favorable and unfavorable conditions lies in the presence of near-surface interactions, we hypothesize that α primarily drives deviations from the favorable RP shape.

In this study, we aim to extend our theoretical framework to incorporate two potential scenarios for α as a function of the number of preceding interceptions: (i) a constant α across interceptions and (ii) a variable α across interceptions. The first scenario, in which α remains constant, has been observed in colloid trajectory simulations under unfavorable conditions [3, 33]. Additionally, we propose an alternative scenario in which α varies as a function of successive interceptions. While introducing a variable α as a function of successive interceptions was previously proposed [33], its impact has not been fully explored. To this end, we seek to develop a theoretical framework capable of accounting for both cases, with the objective of explaining the non-exponential RP shapes that arise under unfavorable conditions. A discussion of potential mechanisms underlying the variability of α with interceptions is provided in §4. Regardless of whether α is constant or variable, the overall retention profile is governed by a gamma distribution, arising from the summation of exponential distributions across multiple interceptions [3, 33].

2.3.1 Including Constant α with Interceptions

We begin with the first scenario, in which a constant fraction is removed from the bulk in which α is constant across all interception orders. Figure 2, panel a, illustrates a schematic of the process of upscaling from the single-interception scale to Darcy scale. Figure 2, panel b, depicts the removal process occurring at each interception order. Here, a constant fraction α of the intercepted colloids is removed at each interception. The remaining fraction, $1 - \alpha$, returns to the bulk fluid and begins a new trip toward subsequent interceptions. Based on the process depicted in Figure 2, panel b, the number of attached colloids after the nth

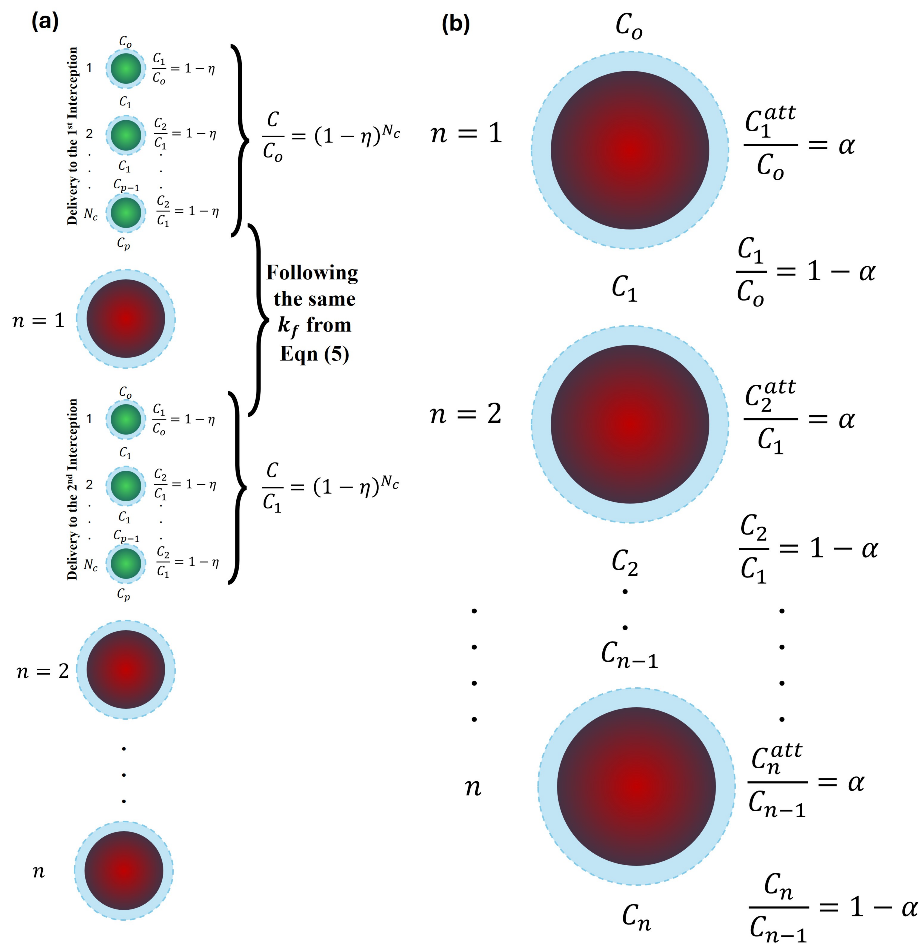

Figure 2: Upscaling strategy from the single-interception scale to the Darcy scale: (a) Schematic illustrating the upscaling process from the grain scale to the Darcy scale via the interception scale. (b) Removal process at each interception, assuming a fraction (α) is removed from the bulk fluid per interception.

interception (C_n^{att}) and the number of colloids returning to the bulk fluid after n interceptions (C_n) are determined using Eqns (6) and (7), respectively.

$$C_n^{att} = C_o \alpha \left(1-\alpha\right)^{n-1} \tag{6}$$

$$C_n = C_o \left(1-\alpha\right)^{n} \tag{7}$$

Figure 2, panel a, illustrates the delivery process to the NSZ over n interceptions. This process is characterized by a sequence of exponential distributions, each governed by a rate constant k_f. The summation of these exponential distributions across multiple interceptions yields a gamma distribution with a shape parameter corresponding to the number of interceptions (n) and a rate constant (k_f), as described in Eqn (5). Consequently, the spatial distribution of attached colloids during the nth interception ($C^{att}(x,n)$) can be expressed using the following Gamma function:

$$\frac{C^{att}(x,n)}{C_n^{att}} = \frac{\left(\frac{k_f}{\langle v\rangle}x\right)^{n-1}}{(n-1)!}\exp\left(-\frac{k_f}{\langle v\rangle}x\right). \tag{8}$$

Substituting Eqn (6) into Eqn (8) yields:

$$C^{att}(x,n) = \frac{\left(\frac{(1-\alpha)k_f}{\langle v\rangle}x\right)^{n-1}}{(n-1)!}\alpha C_o \exp\left(-\frac{k_f}{\langle v\rangle}x\right). \tag{9}$$

Equation (9) describes the spatial distribution of attached colloids during the nth interception order, expressed as a function of k_f and α. Importantly, summing Equation (9) over a large number of interceptions (N_i) yields the RP function, which represents the cumulative number of attached colloids across all interceptions at each spatial location. This cumulative distribution is denoted as $C^{att}(x)$. To derive the complete RP function, the summation of Equation (9) over N_i is performed such that

$$C^{att}(x) = \alpha C_o \exp\left(-\frac{k_f}{\langle v\rangle}x\right)\sum_{n=1}^{N_i}\frac{\left(\frac{(1-\alpha)k_f}{\langle v\rangle}x\right)^{n-1}}{(n-1)!}. \tag{10}$$

Considering all possible attachments, that is taking the limit $N_i \to \infty$, and recognizing the Taylor expansion $e^B = \sum_{m=0}^{\infty}\frac{B^m}{(m)!}$, Eqn (10) can be simplified to

$$C^{att}(x) = \alpha C_o \exp\left(-\frac{\alpha k_f}{\langle v\rangle}x\right), \tag{11}$$

Equation (11) can be directly applied to construct a complete RP under both favorable and unfavorable conditions. Under favorable conditions, where $\alpha \approx 1$, Equation (11) simplifies to Equation (1). On the other hand, under unfavorable conditions ($\alpha \ll 1$), assuming that α remains constant throughout the interceptions, Equation (11) indicates that the resulting RP follows an exponential distribution with a shallower of $\alpha k_f/\langle v\rangle$, compared to the favorable slope ($k_f/\langle v\rangle$) as arrived at by classical CFT.

2.3.2 Including Variable α with Interceptions

As discussed in §2.3.1, the transport of colloidal particles under unfavorable conditions can be modeled as a series of successful interceptions characterized by an attachment rate k_f and a constant fractional removal per interception, α. This framework results in exponential RPs with a reduced effective rate (αk_f) compared to the rate observed under favorable conditions (k_f). While Eqn 11 effectively describes exponential RPs, it is inadequate for capturing the anomalous transport behaviors that manifest in multi-exponential and nonmonotonic shapes.

We hypothesize that a varying α across interceptions, rather than a constant value, may contribute to the emergence of non-exponential RPs under unfavorable conditions. To incorporate variable α, we follow the upscaling in Figure 2, panel b, allowing α_j to vary across interceptions, where α_j represents the attachment fraction at interception j. Thus, after n interceptions, C_n^{att} and C_n can be represented by Eqns (12) and (13), respectively, as

$$C_n^{att} = C_o\alpha_n\prod_{j=1}^{n}\left(1-\alpha_{j-1}\right), \tag{12}$$

$$C_n = C_o\prod_{j=1}^{n}\left(1-\alpha_j\right), \tag{13}$$

where $\prod$ denotes the product operator. Substituting Eqn (12) into the Gamma function represented by Eqn (8) and following the same steps outlined in §2.3.1 and subsequently rearranging the terms yields:

$$C^{att}(x) = C_o \exp\left(-\frac{k_f}{\langle v\rangle}x\right)\sum_{n=1}^{N_i}\left(\frac{\left(\frac{k_f}{\langle v\rangle}x\right)^{n-1}}{(n-1)!}\alpha_n\prod_{j=1}^{n}(1-\alpha_{j-1})\right). \tag{14}$$

This final form of the RP function in Eqn 14 can capture anomalous RP shapes (i.e., multi-exponential and nonmonotonic shapes) by accounting for a variable α across interceptions. Importantly, assuming a constant α across interceptions in Eqn (14) simplifies the terms, ultimately leading to Eqn (11). Therefore, Eqn (14) serves as the general expression applicable to both variable and constant α across interceptions.

To investigate the impact of a variable α across interceptions on the RP slope near the inlet, which is critical in determining whether the RP shape is multi-exponential or non-monotonic, we ask whether the expression in Eqn 14 can even yield such results. One critical feature in determining this is whether the slope of $C^{att}(x=0)$ can be either negative (exponential or multi-exponential) or positive (non-monotonic) and what conditions must be met to influence this. In calculating this slope it is sufficient to only focus on the first two interceptions in Eqn (14); higher-order interceptions are negligible, as third and higher-level interceptors do not attach near the inlet. As noted, we calculate the slope of the RP $(dC^{att}(x)/dx)$ at $x=0$:

$$\left.\frac{dC^{att}(x)}{dx}\right|_{x=0} = C_o\frac{k_f}{\langle v\rangle}\left(\alpha_2\left(1-\alpha_1\right)-\alpha_1\right). \tag{15}$$

The sign of Equation (15) determines the slope of the RP near the inlet. This implies that changes in α within the first few interceptions can potentially account for non-exponential RP shapes. As indicated by Eqn (15), when $\alpha_2 > \alpha_1/\left(1-\alpha_1\right)$, the RP slope near the inlet will be positive, resulting in a non-monotonic RP. By contrast, when $\alpha_2 < \alpha_1/\left(1-\alpha_1\right)$, the RP slope near the inlet will be negative, leading to exponential or multi-exponential RPs. Therefore, the key factor governing the RP slope near the inlet is whether α_2 exceeds or falls below $\alpha_1/\left(1-\alpha_1\right)$. Notably, the term $\alpha_1/\left(1-\alpha_1\right)$ exceeds unity when $\alpha_1 \geq 0.5$. Given that α at any interception is constrained between 0 and 1, the RP slope near the inlet, as described by Equation (15), remains negative (exponential or multi-exponential) for all values of α_2 if $\alpha_1 \geq 0.5$. More broadly, if $\alpha_1 \geq 0.5$, the RP is expected to exhibit exponential or multi-exponential characteristics. However, when $\alpha_1 < 0.5$, the term $\alpha_1/\left(1-\alpha_1\right)$ is less than 1, in which case the RP slope near the inlet may be either positive or negative, depending on the value of α_2.

3 Model Validation

In this section, we validate our theoretical framework by evaluating its performance under both favorable and unfavorable conditions, leveraging benchmark simulations from [3]. These simulations include RPs generated across various degrees of favorability using The One Piece Model for Particle Tracking [1]. Under unfavorable conditions, the simulations incorporate heterodomains on the collector surfaces, with the favorability quantified by the fraction of the collector surface occupied by heterodomains, referred to as SCOV. The simulations were conducted over a 2D domain consisting of uniform grains with a size of 200 μm (d_c), a porosity of 0.54 (ϵ), and identical colloids of 1.1 μm in size (d_p). Further details regarding the governing equations of the simulations and the DLVO parameters can be found in [2, 3]. Table 1 summarizes the benchmark simulations used for our model validation, listing the corresponding values of SCOV, $\langle v\rangle$, η, k_f, and α for each case.

For scenarios where α remains constant across interceptions, RPs can be determined using Eqn (11), which depends on the values of $\langle v\rangle$, k_f, and α under favorable and unfavorable

Table 1: Summary of cases are used in the model validation [3]

Case No.	**SCOV%**	$\langle v \rangle$ **[m/day]**	η^a	k_f^b **[1/s]**	α
C1	100	4.27	0.0084	0.0024	0.96^c
C2	0.45	4.27	0.0084	0.0024	0.25^c
C3	0.23	4.27	0.0084	0.0024	0.13^c
C4	0.15	4.27	0.0084	0.0024	0.11^c
C5	0.15	2.13	0.0136	0.0020	0.11^c
C6	0.15	8.54	0.0052	0.0030	0.11^c
C7	0.15	4.27	0.0084	0.0024	$f_\alpha(n)^d$
C8	0.15	4.27	0.0084	0.0024	$g_\alpha(n)^d$

[a] Calculated using correlation equations from [22]. [b] Calculated using Eqn (5). [c] A constant value with encountered interceptions, calculated from pore-assembly trajectory simulations [3]. [d] Function of number of interceptions (n), synthetically adopted from case 4 and presented in Figure (4), panel a.

conditions. Since variations in SCOV influence only the near-surface attachment (governed by α), the parameters $\langle v \rangle$ and k_f remain unaffected when SCOV changes. The first four cases in Table 1, labeled C1–C4, represent scenarios where only SCOV varies, leading to changes in α while $\langle v \rangle$ and k_f remain the same. By substituting the values from Table 1 for cases C1–C4 into Eqn (11), the corresponding RPs under both favorable and unfavorable conditions are computed. These results are compared with the benchmark simulations in Figure (3), panel a. The outcomes illustrated in Figure 3, panel a, demonstrate strong agreement between the simulated RPs and those estimated using our analytical model under all tested conditions. Additionally, Figure 3, panel b, shows agreement between the benchmark simulations and our analytical model for cases with similar α but different k_f, highlighting the influence of changes in $\langle v \rangle$ (Cases C4, C5, and C6). These findings underscore the robustness of the analytical model in capturing RPs accurately under both favorable and unfavorable conditions. Consequently, the model serves as a reliable tool for interpreting colloid transport and retention dynamics across a range of environmental conditions.

Although Eqn (11) is effective in generating exponential RPs under both favorable and unfavorable conditions, it is inadequate for describing the non-exponential anomalous RPs observed experimentally under unfavorable conditions [19, 20]. To address this limitation, Eqn (14) introduces a variable α as a function of the number of encountered interceptions. This modification breaks the exponential RP shape, yielding multi-exponential or nonmonotonic profiles depending on whether α increases or decreases with interceptions. To examine the impact of varying α, parameters from Case C4 are used to create Cases C7 and C8, as summarized in Table 1. The key distinction between Cases C7 and C8 and Case C4 lies in the variation of α with interceptions. In Case C7, α initially decreases with interceptions before stabilizing at a constant value of 0.11, as in Case C4. This is intended to reflect some pre-asymptotic behavior that stabilizes to an asymptotic one, consistent with the fact that at a large distance from the inlet in experiments both multi-exponential and non-monotonic profiles converge to a single rate exponential behavior. Conversely, in Case C8, α initially increases with interceptions and subsequently reaches the same constant value of 0.11. These variations in α are illustrated in Figure 4, panel a. Using the variable α functions from Figure 4, panel a, for Cases C7 and C8 in Eqn (14) generates anomalous RPs, multi-exponential and nonmonotonic shapes, as shown in Figure 4, panel b. These findings demonstrate that Eqn (14) can effectively captures anomalous RP behaviors observed under unfavorable conditions by incorporating a variable α as a function of the number of interceptions. This approach

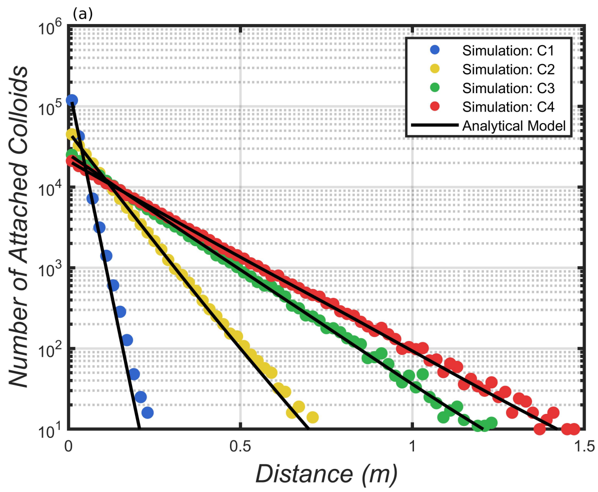

Figure 3: Constant α - Validation of the analytical model against benchmark simulations from [3] under favorable and unfavorable conditions using colloids with a diameter d_p of 1.1 μm. (a) Cases C1 (favorable: SCOV of 100%) through C4 (unfavorable: SCOV of 0.15%) demonstrate varying SCOV values, leading to different α values for each case, while the value of k_f remains constant across all cases, unaffected by SCOV. (b) Unfavorable cases C4 through C6, with a constant SCOV of 0.15%, highlight different $\langle v \rangle$ values, resulting in different k_f values for each case, while α remains constant across all cases, unaffected by $\langle v \rangle$.

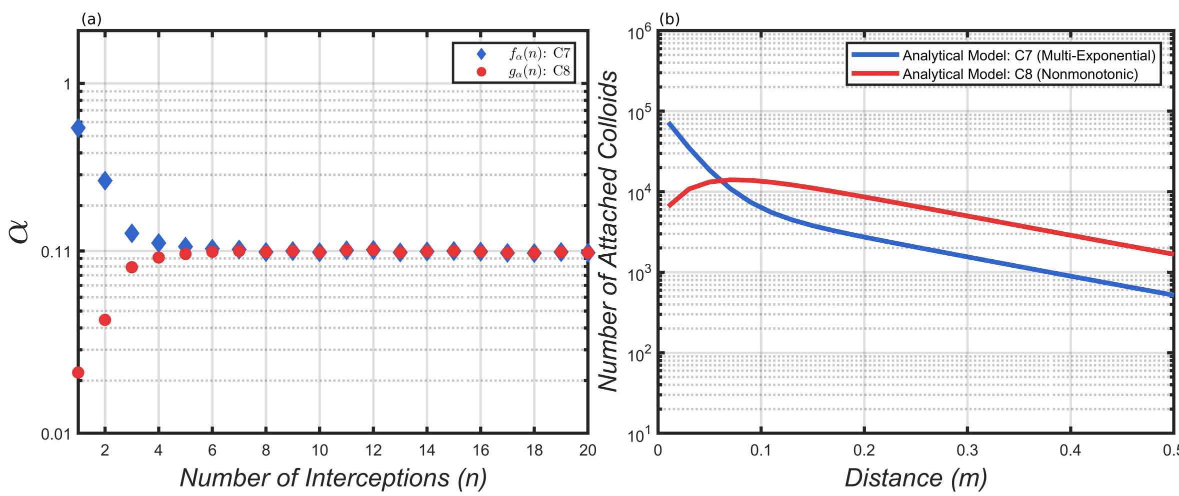

Figure 4: Variable α - Generation of anomalous RPs shapes under unfavorable conditions (cases: C7 and C8) using our analytical model with synthetically defined α that either initially increases or decreases with the number of encountered interceptions (n). (a) The α values as functions of the number of interceptions for cases where α initially decreases ($f_\alpha(n)^d$) and where it initially increases ($g_\alpha(n)^d$). (b) Creation of anomalous multi-exponential and non-monotonic RPs for cases C7 and C8, respectively, using our analytical model with synthetic α data, described in panel a, illustrating the impact of variable α on the shape of the RPs.

enables the representation of multi-exponential and nonmonotonic behaviors, aligning the suggested analytical model with observed experimental trends. At this stage, these changes in α are synthetically created to demonstrate the effect of varying α. Still, we are actively exploring what can give rise to these changes in real settings and discuss possible reasons in the following section.

4 Discussion - Why α Could Change Across Interceptions?

Colloid transport and retention in porous media are governed by two distinct processes: (i) the physics of delivery in the bulk fluid to the NSZ and (ii) the physics governing interactions within the NSZ [3, 33]. Uniform values of k_f (or η) and α throughout the transport domain will yield an invariant RP shape, resulting in an exponential profile, as depicted in Figure (3). However, based on Eqns (11) and (14), either k_f, α, or both must exhibit spatial variation, particularly near the inlet, to produce non-exponential RPs. While the spatial variation of α is primarily driven by the physics inside the NSZ, k_f is less likely to vary across the transport domain due to its dependence on bulk fluid delivery, which remains unaffected by the degree of favorability. Nonetheless, localized variations in k_f near the inlet may arise due to initial injection conditions [2]. However, this effect is expected to diminish downstream after a few grains, particularly in the 2D geometry used in their study, and is not expected to be as significant as varying α. Given these considerations, we propose that spatial variability in α constitutes a plausible, although not necessarily exclusive, mechanism for explaining the emergence of non-exponential RP shapes.

Within the NSZ, α is governed by the total interaction potential, encompassing surface charge heterogeneity, DLVO interactions, extended DLVO interactions, and non-DLVO interactions. Having a value of α less than unity can be interpreted as indicative of a reaction-limited system, wherein the attachment rate is lower than the maximum rate attainable in the absence of a repulsive barrier under favorable conditions. While these conditions primarily determine the magnitude of α, their spatial variation governs the spatial variability of α, rather than their localized effects at specific spatial locations. Therefore, it is essential to examine whether spatial variations in DLVO interactions or surface charge heterogeneity contribute to the observed variability in α. First, DLVO forces are strongly dependent on the material properties of the fluid, grains, and colloids. Consequently, any spatial variation in these properties would manifest as spatial variation in α. Theoretically, variations in the distribution of surface charge heterogeneity can potentially justify the spatial variability in α. However, not all DLVO parameters contribute equally to this variation, as certain parameters are more sensitive to changes in the system's physical and chemical conditions than others.

Additionally, incomplete pore-scale mixing near the inlet can naturally induce spatial variations in the physicochemical properties of the system. Such incomplete mixing and pre-asymptotic effects naturally give rise to what appear like anomalous behaviors that given enough time/distance wash out initial and boundary conditions effects [6, 30]. Incomplete mixing, in the context of solutes, goes through a series of behaviors reflecting initial lamellar stretching, coalescence, and then asymptotic dispersion [7, 8, 17, 18], and each of these may persist for longer given the significantly lower diffusion coefficient of colloids relative to a solute. The earliest stages, particularly for high Peclet numbers, can lead to very extended regions of incomplete mixing and although this stage evolves quickly over only a few grain lengths its signature persists over large distances [9, 21]. While theoretical analyses suggest that variations in material properties or surface charge heterogeneity could account for spatial variations in α, such effects are unlikely under the controlled conditions commonly used in colloid transport experiments. Instead, incomplete mixing near the inlet provides a possible plausible explanation for these variations. This phenomenon occurs over short distances and can disrupt the uniform distribution of colloids and solutes, thereby impacting interactions between colloids and grain surfaces. Such disruptions may lead to localized differences in attachment behavior and transport dynamics. By modifying the physical and chemical environment near the inlet, incomplete pore-scale mixing might significantly contribute to the spatial variability of the system's properties.

The primary objective of this study is to establish a novel theoretical framework capable of capturing both exponential and anomalous (non-exponential) RP shapes under favorable and unfavorable conditions. Our model demonstrates that a constant α across interceptions yields exponential RPs, whereas spatially varying α enables multi-exponential and nonmonotonic behaviors. While prior mechanistic trajectory simulations have confirmed that a constant α with interceptions can occur [3, 33], we speculate that α can vary to explain the emergence of non-exponential RP shapes under unfavorable conditions. Thus, this study focuses on developing the theoretical basis sufficient to describe the anomalous RPs when α varies across interceptions without attempting to provide a quantitative characterization of its spatial variation. In summary, while the detailed mechanisms driving the spatial variation of α fall beyond the specific scope of this study, we propose that the interplay of surface charge heterogeneity, spatially varying DLVO interactions, and incomplete pore-scale mixing likely underlies the spatial variation in α and will dedicate future efforts to explore and understand this potential variability in greater detail. While a recent experimental study ([14]) has reported an increase in α across interception orders, a more detailed investigation of potential drivers for such variation will be the subject of future work (e.g., [4]).

5 Conclusion

In this study, we have developed a novel theoretical model to upscale colloid transport from grain scale to Darcy scale under favorable and unfavorable conditions. By incorporating colloid interception history, the model not only captures traditional exponential RPs but also accounts for anomalous, non-exponential behaviors under unfavorable conditions. The proposed model demonstrates that if k_f and α remain constants across the transport domain, RPs must exhibit exponential forms even under unfavorable conditions, though with a shallower slope of $\alpha k_f/\langle v\rangle$ compared to the favorable slope of $k_f/\langle v\rangle$, as outlined by the classical CFT.

A key innovation of this work is the development of the model to account for variable α that changes with the number of interceptions. This modification enables the model to produce multi-exponential and nonmonotonic retention profiles, which are commonly observed in experimental settings under unfavorable conditions. The ability to represent these anomalous behaviors expands the model's applicability to a broader range of environmental conditions, particularly in systems where traditional exponential decay does not hold. Although this study speculates on how α may vary across interceptions, considering factors such as incomplete pore-scale mixing, spatial variability of DLVO interactions, and surface charge heterogeneity, it emphasizes the need for further research into the spatial variability of α. This opens the door for future investigations to better understand the underlying mechanisms contributing to these variations.

The strength of the model lies in its simplicity and versatility, enabling its application to a wide range of scenarios, regardless of the complexity of the underlying surface interactions or the nature of colloidal transport. By incorporating the influence of changing α among interceptions, the model offers an accurate representation of colloid behavior in natural systems, where conditions often deviate from idealized exponential assumptions.

Acknowledgments

This work was supported by US National Science Foundation projects EAR-1951676 and EAR-1951677.

Author Contributions

BMA: Conceptualization, Methodology, Writing—Original Draft, Writing—Review & Editing, Visualization.
WPJ: Conceptualization, Methodology, Writing—Review & Editing, Funding acquisition.
DB: Conceptualization, Methodology, Writing—Original Draft, Writing—Review & Editing, Funding acquisition.

Open Research

The particle tracking model used in this manuscript for the calculation of the RPs is licensed under MIT license and published on Github: https://github.com/BasharAlZghoul/The-One-Piece-for-Particle-Tracking [1]

References

[1] Bashar M Al-Zghoul, William P Johnson, and Diogo Bolster. The One Piece for Particle Tracking [Software]. 11 2023. doi: 10.5281/zenodo.10068085.

[2] Bashar M. Al-Zghoul, Sabrina N. Volponi, W. P. Johnson, and Diogo Bolster. Effects of Initial Injection Condition on Colloid Retention. *Water Resources Research*, 60(6), 6 2024. ISSN 19447973. doi: 10.1029/2023WR036877.

[3] Bashar M. Al-Zghoul, William P. Johnson, and Diogo Bolster. A training trajectory random walk model for upscaling colloid transport under favorable and unfavorable conditions. *Advances in Water Resources*, page 104878, 1 2025. ISSN 03091708. doi: 10.1016/j.advwatres.2024.104878.

[4] Bashar M Al-Zghoul, William P Johnson, Luis Ullauri, and Diogo Bolster. Parameters Driving Anomalous Transport in Colloids: Dimensional Analysis (In Review). *Langmuir*, 2025.

[5] Otto Albinger, Brian K Biesemeyer, Robert G Arnold, and Bruce E Logan. Effect of bacterial heterogeneity on adhesion to uniform collectors by monoclonal populations. Technical report, 1994.

[6] Diogo Bolster, Alice Hang, and P. F. Linden. The front speed of intrusions into a continuously stratified medium. *Journal of Fluid Mechanics*, 594:369–377, 1 2008. ISSN 14697645. doi: 10.1017/S0022112007008993.

[7] Pietro De Anna, Marco Dentz, Alexandre Tartakovsky, and Tanguy Le Borgne. The filamentary structure of mixing fronts and its control on reaction kinetics in porous media flows. *Geophysical Research Letters*, 41(13):4586–4593, 7 2014. ISSN 19448007. doi: 10.1002/2014GL060068.

[8] Pietro De Anna, Joaquin Jimenez-Martinez, Hervé Tabuteau, Regis Turuban, Tanguy Le Borgne, Morgane Derrien, and Yves Méheust. Mixing and reaction kinetics in porous media: An experimental pore scale quantification. *Environmental Science and Technology*, 48(1):508–516, 1 2014. ISSN 15205851. doi: 10.1021/es403105b.

[9] Saif Farhat, Guillem Sole-Mari, Daniel Hallack, and Diogo Bolster. Evolution of pore-scale concentration PDFs and estimation of transverse dispersion from numerical porous

media column experiments. *Advances in Water Resources*, 191, 9 2024. ISSN 03091708. doi: 10.1016/j.advwatres.2024.104770.

[10] W. P. Johnson and E. Pazmiño. *Colloid (Nano- and Micro-Particle) Transport and Surface Interaction in Groundwater*. The Groundwater Project, 2023. ISBN 9781774700709. doi: 10.21083/978-1-77470-070-9.

[11] W. P. Johnson, A. Rasmuson, E. Pazmiño, and M. Hilpert. Why Variant Colloid Transport Behaviors Emerge among Identical Individuals in Porous Media When Colloid-Surface Repulsion Exists. *Environmental Science and Technology*, 52(13):7230–7239, 7 2018. ISSN 15205851. doi: 10.1021/acs.est.8b00811.

[12] William P. Johnson. Quantitative Linking of Nanoscale Interactions to Continuum-Scale Nanoparticle and Microplastic Transport in Environmental Granular Media. *Environmental Science and Technology*, 54(13):8032–8042, 7 2020. ISSN 15205851. doi: 10.1021/acs.est.0c01172.

[13] William P. Johnson and Markus Hilpert. Upscaling colloid transport and retention under unfavorable conditions: Linking mass transfer to pore and grain topology. *Water Resources Research*, 49(9):5328–5341, 9 2013. ISSN 19447973. doi: 10.1002/wrcr.20433.

[14] William P Johnson, Luis Ullauri, Bashar M Al-Zghoul, and Diogo Bolster. Experimental Confirmation of the Interception History Paradigm for Colloid (Micro and Nano Particle) Transport in Porous Media. *Environmental Science & Technology (In Review)*, 2025.

[15] Tamir Kamai, Mohamed K. Nassar, Kirk E. Nelson, and Timothy R. Ginn. Colloid filtration prediction by mapping the correlation-equation parameters from transport experiments in porous media. *Water Resources Research*, 51(11):8995–9012, 11 2015. ISSN 19447973. doi: 10.1002/2015WR017403.

[16] Ruben Kretzschmar, Kurt Barmettler, Daniel Grolimund, Yao De Yan, Michal Borkovec, and Hans Sticher. Experimental determination of colloid deposition rates and collision efficiencies in natural porous media. *Water Resources Research*, 33(5):1129–1137, 1997. ISSN 00431397. doi: 10.1029/97WR00298.

[17] T. Le Borgne, M. Dentz, and E. Villermaux. The lamellar description of mixing in porous media. *Journal of Fluid Mechanics*, 770:458–498, 5 2015. ISSN 14697645. doi: 10.1017/jfm.2015.117.

[18] Tanguy Le Borgne, Marco Dentz, Philippe Davy, Diogo Bolster, Jesus Carrera, Jean Raynald De Dreuzy, and Olivier Bour. Persistence of incomplete mixing: A key to anomalous transport. *Physical Review E - Statistical, Nonlinear, and Soft Matter Physics*, 84(1), 7 2011. ISSN 15502376. doi: 10.1103/PhysRevE.84.015301.

[19] Xiqing Li and William P. Johnson. Nonmonotonic variations in deposition rate coefficients of microspheres in porous media under unfavorable deposition conditions. *Environmental Science and Technology*, 39(6):1658–1665, 3 2005. ISSN 0013936X. doi: 10.1021/es048963b.

[20] Xiqing Li, Timothy D. Scheibe, and William P. Johnson. Apparent decreases in colloid deposition rate coefficients with distance of transport under unfavorable deposition conditions: A general phenomenon. *Environmental Science and Technology*, 38(21):5616–5625, 11 2004. ISSN 0013936X. doi: 10.1021/es049154v.

[21] Daniel M C Hallack, Guillem Sole-Mari, Saif Farhat, and Diogo Bolster. 3D Pore-Scale Mixing Interface Evolution. *ARC Geophysical Research*, 1(1), 1 2025. doi: 10.5149/ARC-GR.1294.

[22] Huilian Ma, Julien Pedel, Paul Fife, and William P. Johnson. Hemispheres-in-cell geometry to predict colloid deposition in porous media. *Environmental Science and Technology*, 43(22):8573–8579, 11 2009. ISSN 0013936X. doi: 10.1021/es901242b.

[23] Ian L. Molnar, William P. Johnson, Jason I. Gerhard, Clinton S. Willson, and Denis M. O'Carroll. Predicting colloid transport through saturated porous media: A critical review, 9 2015. ISSN 19447973.

[24] Kirk E. Nelson and Timothy R. Ginn. New collector efficiency equation for colloid filtration in both natural and engineered flow conditions. *Water Resources Research*, 47 (5), 2011. ISSN 00431397. doi: 10.1029/2010WR009587.

[25] Eddy Pazmino, Jacob Trauscht, Brittany Dame, and William P. Johnson. Power law size-distributed heterogeneity explains colloid retention on soda lime glass in the presence of energy barriers. *Langmuir*, 30(19):5412–5421, 5 2014. ISSN 15205827. doi: 10.1021/la501006p.

[26] Rajamani Rajagopalan and Chi Tien. Trajectory analysis of deep-bed filtration with the sphere-in-cell porous media model. *AIChE Journal*, 22(3):523–533, 1976. ISSN 15475905. doi: 10.1002/aic.690220316.

[27] Cesar A. Ron, Kurt Vanness, Anna Rasmuson, and William P. Johnson. How nanoscale surface heterogeneity impacts transport of nano- to micro-particles on surfaces under unfavorable attachment conditions. *Environmental Science: Nano*, 6(6):1921–1931, 2019. ISSN 20518161. doi: 10.1039/c9en00306a.

[28] Joseph N Ryan and Menachem Elimelech. COLLOIDS A AND Colloids and Surfaces SURFACES ELSEVIER Colloid mobilization and transport in groundwater. Technical report, 1996.

[29] Eleanor Spielman-Sun, Kristin Boye, Dipankar Dwivedi, Maya Engel, Aaron Thompson, Naresh Kumar, and Vincent Noël. A Critical Look at Colloid Generation, Stability, and Transport in Redox-Dynamic Environments: Challenges and Perspectives, 4 2024. ISSN 24723452.

[30] Wilson L. Taylor. "Cloze Procedure": A New Tool for Measuring Readability. *Journalism Quarterly*, 30(4):415–433, 9 1953. ISSN 0022-5533. doi: 10.1177/107769905303000401.

[31] Meiping Tong and William P. Johnson. Colloid population heterogeneity drives hyperexponential deviation from classic filtration theory. *Environmental Science and Technology*, 41(2):493–499, 1 2007. ISSN 0013936X. doi: 10.1021/es061202j.

[32] Nathalie Tufenkji and Menachem Elimelech. Spatial distributions of Cryptosporidium oocysts in porous media: Evidence for dual mode deposition. *Environmental Science and Technology*, 39(10):3620–3629, 5 2005. ISSN 0013936X. doi: 10.1021/es048289y.

[33] Sabrina N. Volponi, Bashar M. Al-Zghoul, Giovanni Porta, Diogo Bolster, and William P. Johnson. Interception History Drives Colloid Transport Variance in Porous Media. *Environmental Science & Technology*, 2 2025. ISSN 0013-936X. doi: 10.1021/acs.est.4c06509.

[34] Sabrina N. Volponi, Giovanni Porta, Bashar Al-Zghoul, Diogo Bolster, and William P. Johnson. Inferring experimental colloid removal with an inverse two-population model linking continuum scale data to nanoscale features. *Advances in Water Resources*, page 104905, 1 2025. ISSN 03091708. doi: 10.1016/j.advwatres.2025.104905.

[35] Kuan-Mu Yao, Mohammad T. Habibian, and Charles R. O'Melia. Water and waste water filtration. Concepts and applications. *Environmental Science & Technology*, 5(11): 1105–1112, 11 1971. ISSN 0013-936X. doi: 10.1021/es60058a005.